Check for updates

RESEARCH ARTICLE

REVISED Synthesis and physical characteristics of narrow bandgap chalcogenide $SnZrSe_3$

[version 2; peer review: 2 approved]

Rokas Kondrotas[1], Remigijus Juškėnas[1], Arūnas Krotkus[1], Vidas Pakštas[1], Artūras Suchodolskis[1], Algirdas Mekys[2], Marius Franckevičius[1], Martynas Talaikis[1], Katri Muska[3], Xiaofeng Li[3], Marit Kauk-Kuusik[3], Victor Kravtsov[4]

[1]Center for Physical Sciences and Technology, Vilnius, 10257, Lithuania
[2]Institute of Photonics and Nanotechnology, Vilnius University, Vilnius, 10257, Lithuania
[3]Department of Materials and Environmental Technology, Tallinn University of Technology, Tallinn, 19086, Estonia
[4]Institute of Applied Physics, Chisinau, MD2028, Moldova

v2 **First published:** 13 Dec 2022, **2**:138
https://doi.org/10.12688/openreseurope.15168.1
Latest published: 17 May 2023, **2**:138
https://doi.org/10.12688/openreseurope.15168.2

Abstract

Background: The development of organic/inorganic metal halide perovskites has seen unprecedent growth since their first recognition for applications in optoelectronic devices. However, their thermodynamic stability and toxicity remains a challenge considering wide-scale deployment in the future. This spurred an interest in search of perovskite-inspired materials which are expected to retain the advantageous material characteristics of halide perovskites, but with high thermodynamic stability and composed of earth-abundant and low toxicity elements. ABX_3 chalcogenides (A, B=metals, X=Se, S) have been identified as potential class of materials meeting the aforementioned criteria.
Methods: In this work, we focus on studying tin zirconium selenide ($SnZrSe_3$) relevant physical properties with an aim to evaluate its prospects for application in optoelectronics. $SnZrSe_3$ powder and monocrystals were synthesized via solid state reaction in 600 – 800 °C temperature range. Crystalline structure was determined using single crystal and powder X-ray diffraction methods. The bandgap was estimated from diffused reflectance measurements on powder samples and electrical properties of crystals were analysed from temperature dependent *I-V* measurements.
Results: We found that $SnZrSe_3$ crystals have a needle-like structure (space group – *Pnma*) with following unit cell parameters: a=9.5862(4) Å, b=3.84427(10) Å, c=14.3959(5) Å. The origin of the low symmetry crystalline structure was associated with stereochemical active electron lone pair of Sn cation. Estimated bandgap was around 1.15 eV which was higher than measured previously and predicted theoretically. Additionally, it was found that resistivity and conductivity

Open Peer Review

Approval Status ✓ ✓

	1	2
version 2 (revision) 17 May 2023	✓ view	
version 1 13 Dec 2022	? view	✓ view

1. **Hao Zeng**, University at Buffalo, Buffalo, USA

2. **Yi-Yang Sun**, Shanghai Institute of Ceramics, Chinese Academy of Science, Shanghai, China

Any reports and responses or comments on the article can be found at the end of the article.

type depended on the compound chemical composition.
Conclusions: Absorption edge in the infrared region and bipolar dopability makes $SnZrSe_3$ an interesting material candidate for application in earth-abundant and non-toxic single/multi-junction solar cells or other infrared based optoelectronic devices.

Keywords
ABX3 chalcogenides, crystal structure, optoelectronic properties, bandgap

This article is included in the Marie-Sklodowska-Curie Actions (MSCA) gateway.

This article is included in the Horizon 2020 gateway.

This article is included in the Inorganic Chemistry gateway.

This article is included in the Perovskites collection.

Corresponding author: Rokas Kondrotas (rokas.kondrotas@ftmc.lt)

Author roles: Kondrotas R: Conceptualization, Data Curation, Formal Analysis, Funding Acquisition, Investigation, Project Administration, Resources, Supervision, Validation, Visualization, Writing – Original Draft Preparation, Writing – Review & Editing; **Juškėnas R**: Investigation, Resources, Writing – Review & Editing; **Krotkus A**: Writing – Review & Editing; **Pakštas V**: Investigation; **Suchodolskis A**: Formal Analysis, Investigation; **Mekys A**: Formal Analysis, Investigation; **Franckevičius M**: Investigation, Methodology; **Talaikis M**: Investigation; **Muska K**: Investigation, Writing – Review & Editing; **Li X**: Investigation; **Kauk-Kuusik M**: Resources, Writing – Review & Editing; **Kravtsov V**: Investigation, Resources, Validation, Writing – Review & Editing

Competing interests: No competing interests were disclosed.

Grant information: This project has received funding from the European Union's Horizon 2020 research and innovation programme under the Marie Sklodowska-Curie grant agreement No 895046 (project Chalcopyrite-perovskites for infrared photovoltaics [IRPV]). This research was also supported by projects National Agency for Research and Development (ANCD) 20.80009.5007.15 and TK141 supported by European Union through the European Regional Development Fund, and by the Estonian Research Council under grant agreement No PRG1023.

Copyright: © 2023 Kondrotas R *et al*. This is an open access article distributed under the terms of the Creative Commons Attribution License, which permits unrestricted use, distribution, and reproduction in any medium, provided the original work is properly cited.

How to cite this article: Kondrotas R, Juškėnas R, Krotkus A *et al.* **Synthesis and physical characteristics of narrow bandgap chalcogenide $SnZrSe_3$ [version 2; peer review: 2 approved]** Open Research Europe 2023, **2**:138 https://doi.org/10.12688/openreseurope.15168.2

First published: 13 Dec 2022, **2**:138 https://doi.org/10.12688/openreseurope.15168.1

REVISED **Amendments from Version 1**

The new version of the publication entails:
1. Updated Figure 1 (XRD patterns) and complemented paragraph about solid state reaction and XRD analysis. More experimental evidence were provided on how to obtain higher yield of $SnZrSe_3$ phase.
2. Update on experimental details covering new experiment parameters.
3. Where relevant, elaborated discussions regarding the $SnZrSe_3$ optical properties with respect to its non-perovskite structure.
4. Added three new references.

Any further responses from the reviewers can be found at the end of the article

Plain language summary

The sun provides an enormous amount of energy to the planet and has the potential to meet all humanity power demands. Photovoltaic (PV) technologies, i.e. devices that convert sunlight directly to electricity, play an essential role in harvesting this solar energy. While the sun will shine and provide clean energy for many million years to come, the manufacture of PV technologies uses finite earth resources and depending on the type of technology can be energy demanding and therefore emit large amounts of CO_2. For these reasons, scientists are constantly improving synthesis and fabrication processes to increase material utilization, improving device structure to increase power conversion coefficient and study stability dynamics to prolong device lifetime. In parallel, new materials composed of earth-abundant and non-toxic chemical elements are explored which could potentially replace or complement current technologies. In this work, we focus on investigating a promising compound composed of non-toxic and earth-abundant elements from ABX_3 chalcogenide family materials – $SnZrSe_3$. Using a solid state reaction method, we synthesized $SnZrSe_3$ crystals and measured their optical and electrical properties. We found that a critical semiconductor feature – bandgap (which indicates what wavelength light will be absorbed) of $SnZrSe_3$ is in the suitable range for application in solar cells. Additionally, electrical measurements indicated that $SnZrSe_3$ can be engineered to behave as n- or p-type semiconductor which is very important for the formation of semiconductor devices. In summary, we believe that $SnZrSe_3$ is an interesting candidate for development of greener PV technologies.

Introduction

Perovskite class of materials describe compounds sharing the same type of crystal structure (perovskite) and have specific stoichiometry – ABX_3, where A and B are cations, and X is an anion. The unprecedented development of organic/inorganic lead halide perovskites (HP) for application in light-emitting diodes[1], X-ray detectors[2] and photovoltaics[3] has been witnessed in the last decade. Despite their tremendous success, poor thermodynamic stability under ambient conditions[4] and the presence of a toxic chemical element (Pb)[5] question their wide-scale deployment in the future. This spurred an interest in search of materials with the same advantageous physical properties as HP, but with much higher chemical stability and environmentally benign compositions[6].

The success of HP is thought to be caused by an unusual material property – defect tolerance. This means that despite having a high density of crystallographic defects in the semiconductor, charge carrier lifetime on the order of µs can be readily obtained[7]. However, there is no consensus on the origins of the defect tolerance and it has been associated with multiple material aspects that are characteristic to metal HP, such as: special bonding-antibonding character when antibonding states are at the top of the valence band[8], coordination environment and ionic nature of chemical bonds[6,9], and with a high static dielectric constant effectively screening charged defects[6,10].

When searching for perovskite-inspired materials it is therefore important to know how defect tolerance is related to the structural characteristics of the compound. For instance, it has been proposed that materials comprised of cations with lone electron pairs can potentially have defect tolerance characteristics[10]. Alternatively, a more straightforward way is to explore compounds with perovskite structure and ABX_3 composition. For this reason, and because of high thermodynamic stability, low toxicity and earth-abundant chemical composition, chalcogenide perovskites (X=Se, S) have gained a lot of interest in recent years[11].

The first study on chalcogenide perovskite properties using first-principles calculations was introduced by Sun *et al.*[12] (Note: that the study was limited to chalcogenide composition $A^{2+}B^{4+}X^{2-}_3$, where A=Ca, Sr, Ba; B=Ti, Zr; Hf, X=Se, S). It was shown that chalcogenide perovskites had photovoltaic-relevant properties and some even exceeded well-established materials used in solar cells, showing their great potential in photovoltaics. This sparked an interest in chalcogenide perovskites, of which $BaZrS_3$ has drawn the most attention[13–16]. It was, however, shown that among many ABX_3 chalcogenides, under normal conditions, only very few exist as perovskite structures[17]: $BaZrS_3$, $BaHfS_3$, $SrZrS_3$, $SrHfS_3$, $CaZrS_3$. All of them are wide bandgap (> 1.7 eV) semiconductors, and therefore have a relatively narrow application range in optoelectronics. Other ABX_3 chalcogenides although in a non-perovskite ground phase have bandgaps spanning from near to mid-wavelength infrared regions[12]. Additionally, because valence and conduction bands in edge(face)-sharing ABX_3 chalcogenides are primarily determined by p and d orbitals of X and B elements, respectively, the absorption coefficient is expected to be high as well[18]. Note, however, that lower symmetry crystal structures such as needle-like or $BaNiO_3$ type can lead to indirect optical transitions and therefore higher absorption onset as compared with ABX_3 chalcogenides in perovskite-type structure.

In this work, we focus on examining $SnZrSe_3$ which is predicted to have a narrow ~ 0.65 eV bandgap[19]. $SnZrSe_3$ is composed of low-toxicity and earth-abundant chemical elements and is stable under ambient conditions. Additionally, $SnZrSe_3$ and $SnZrS_3$ are both stable in the needle-like phase suggesting

a full chemical range of miscibility in $SnZrSe_xS_{3-x}$ alloy and therefore a high tuneability of the bandgap. Experimentally estimated bandgaps for $SnZrSe_3$ and $SnZrS_3$ were 0.86 eV and 1.2 – 1.4 eV, respectively, however, the data are available only from one source[20]. Therefore, herein we aim to synthesize and estimate the optical and electrical properties of $SnZrSe_3$ for potential application in infrared-based optoelectronic devices.

$SnZrSe_3$ was synthesized by solid state reaction in a powder form and as monocrystals. $SnZrSe_3$ was found to crystallize in orthorhombic structure with space group *Pnma* as confirmed by single-crystal and powder diffraction methods. The absorption edge was estimated at around 1.15 eV indicating to the narrow bandgap nature of $SnZrSe_3$, but considerably higher than reported before and predicted theoretically. Finally, depending on the chemical composition, $SnZrSe_3$ was found to behave as an *n*- or *p*-type semiconductor highlighting bipolar dopability in $SnZrSe_3$ compound.

Methods

$SnZrSe_3$ samples were synthesized via a solid state reaction method. Elemental precursors comprising Sn (99.995%, AlfaAesar, -100 mesh), Zr (99.5% STREM Chemicals, -50 mesh), Se (99.999%, AlfaAesar, -200 mesh) and SnI_2 (99.99%, SigmaAldrich, -10 mesh) were weighted in an Ar filled glove box. The total mass of the precursor before annealing was 0.5±0.005 g plus 0.01±0.005 g of SnI_2. Then, the precursors were introduced to a quartz ampoule (inner diameter – 8 mm, outer – 10 mm, length – 150 mm) which was capped to protect the precursors from the ambient environment when taken outside the glovebox. Before sealing, all 16 ampoules were degassed for 30 – 60 min under approximately 2 Pa pressure. Four ampoules were immersed in an ultrasonic bath to remove precursors stuck to the quartz walls. Ampoules were sealed under vacuum using a flame from an oxygen and propane gas mixture and the final ampoule length was in the 60 – 80 mm range. First batch of ampoules had a carbonized inner wall to avoid quartz reaction with precursor materials during the synthesis step. However, we did not observe any traces of chemical reactions of precursors with a quartz ampoule and the carbonization step was not used for the rest of the samples.

Ampoules were introduced in the tube furnace, 13 of them in a horizontal and 3 of them in a vertical (placed in ceramic holder) positions at the centre of the heating zone. The heating process included either one or two steps: (i) temperature was raised to the top temperature within 3 – 7 h which was varied in the 600 – 800 °C range and held for 10 – 80 h; (ii) in the second step, the temperature was reduced to 100 – 600 °C within 7 – 60 h, and furnace power was switched off leaving to cool down naturally for a few hours. We found that larger crystals were formed when the temperature was reduced slowly in the second stage, instead of maintaining a high furnace temperature for a prolonged period of time.

Single crystal X-ray data of $SnZrSe_3$ were obtained at 20 °C using an Xcalibur E diffractometer equipped with an Eos CCD space detector (Agilent Technologies) and a monochromatic source of MoK_α radiation (graphite monochromator, Oxford inst.). The data were collected and processed using the program CrysAlisPro (Oxford Diffraction Ltd., Version 1.171.37.35, provided with diffractometer) and were corrected for the Lorentz and polarization effects, and absorption. All calculations to solve the structures and to refine the proposed models were carried out with the SHELXS97[21] and SHELXL2014 software packages[22] (SHELX is free of charge for academic users).

The structure was refined by the full matrix least squares method on F2 with anisotropic displacement parameters using the program SHELXL[21]. Crystallographic data and structure refinement details and geometric parameters are given in CIF file (see *Underlying data*[23]). CIF files were deposited with the Cambridge Crystallographic Data Centre CCDC/ICSD, deposition number CSD 2166561, and can be accessed upon request (https://www.ccdc.cam.ac.uk/).

Powder diffraction was measured using Rigaku diffractometer SmartLab with 9 kW rotating Cu anode in Bragg-Brentano geometry. Before measurements, crystals collected from the ampoule were grinded in an agate mortar. Diffractograms were recorded in the range of 10 to 60 2θ degrees with a scan step of 0.01 degree using linear D/tex ultra detector.

Raman measurements were performed using an inVia Raman microscope (Renishaw, Wotton-under Edge, UK) equipped with the 1800 lines/mm grating and thermoelectrically cooled (-70 °C) CCD camera at 532 nm wavelength excitation. Raman spectrum was taken using a 50x/0.75 NA (Leica) objective lens. Laser power was restricted to 0.05 mW and the integration time was set to 300 s. The Raman frequencies were calibrated using the silicon standard according to the line at 520.7 cm^{-1}.

Diffuse reflectance was measured using Shimadzu UV-3600 two-beam spectrometer equipped with a multi-purpose compartment MPC-3100. Samples were placed in a 60 mm integrating sphere and a barium sulphate target was used for calibration.

Scanning Electron Microscope (SEM) images were taken using Helios Nanolab 650 equipped with a field emission gun. Chemical composition was recorded with an energy dispersive spectrometer (Oxford inst.) embedded in SEM. Before Energy Dispersive X-ray (EDX) measurements were made, calibration using a Cu plate was performed and other parameters such as working distance (5 mm), accelerating voltage (20 kV) and exposure time (30s) were kept constant.

Temperature dependent current-voltage measurements were recorded using a Keithley 6487 picoammeter/voltage source. The sample was placed in a closed helium cycle cryostat (Janis CCS-100/204) and the temperature was controlled via a digital temperature controller. Current-voltage measurements were made from 295 to 100 K with a 10 K temperature step size.

Once the set temperature was reached on the thermocouple, it was waited for 3 min for temperature to equalize on the sample.

All data visualization and processing were performed using OriginPro 2021 version 9.8.0.200 (https://www.originlab.com/index.aspx?go=Products/Origin) and files are accessible in *Underlying data*[23]. Alternatively, data can be treated and analysed using freely available software Labplot (https://labplot.kde.org/). Visualization of crystalline structure was done using freely available software Mercury (https://www.ccdc.cam.ac.uk/solutions/csd-core/components/mercury/).

Results

$SnZrSe_3$ solid state synthesis

$SnZrSe_3$ was synthesized via solid state reaction from precursors in elemental form. Unless stated otherwise, a transport agent (SnI_2) was used to accelerate the reaction and to grow single crystals. In other cases, no additives were introduced. In most of experiments, various shapes, sizes and forms of crystals were present inside an ampoule after annealing indicating formation of secondary phases. By analysing X-ray diffraction (XRD) data we found that in addition to $SnZrSe_3$ phase, one or two of the following binary phases were present: $ZrSe_3$ (ICDD# 03-065-2351), $ZrSe_2$ (ICDD# 04-005-5128) and SnSe (ICDD# 04-009-2257). Based on multiple trials, we noticed that the following experimental parameters had a deciding factor on the phase composition: (i) spatial separation of precursor materials (ii) Se overpressure in the ampoule and (iii) annealing duration. When the ampoule was oriented vertically in the annealing zone, $ZrSe_3$ and traces of SnSe phases were present despite the annealing temperature applied (Figure 1a). Interestingly, the addition of transport agent in a form of SnI_2 did not change the phase composition. This suggested that when precursors were in close proximity, the solid-state reaction was not accelerated or favoured for the formation of $SnZrSe_3$ in the presence of a transport agent. When ampoules were oriented horizontally and precursor powder was spread over a certain length, phase composition strongly depended on the initial Se content. Using Se-deficient precursor, a large amount of $ZrSe_2$ and absence of $ZrSe_3$ phases were observed in the powder (Figure 1b). Once stoichiometric or Se-rich precursors were used, little to no amount of $ZrSe_2$ was found, which indicated that the formation of $ZrSe_3$ phase was highly favoured under Se-rich atmosphere. Note that when the ampoules were oriented horizontally no secondary Sn-related phases were observed. Finally, the annealing duration at the top temperature had a significant effect on

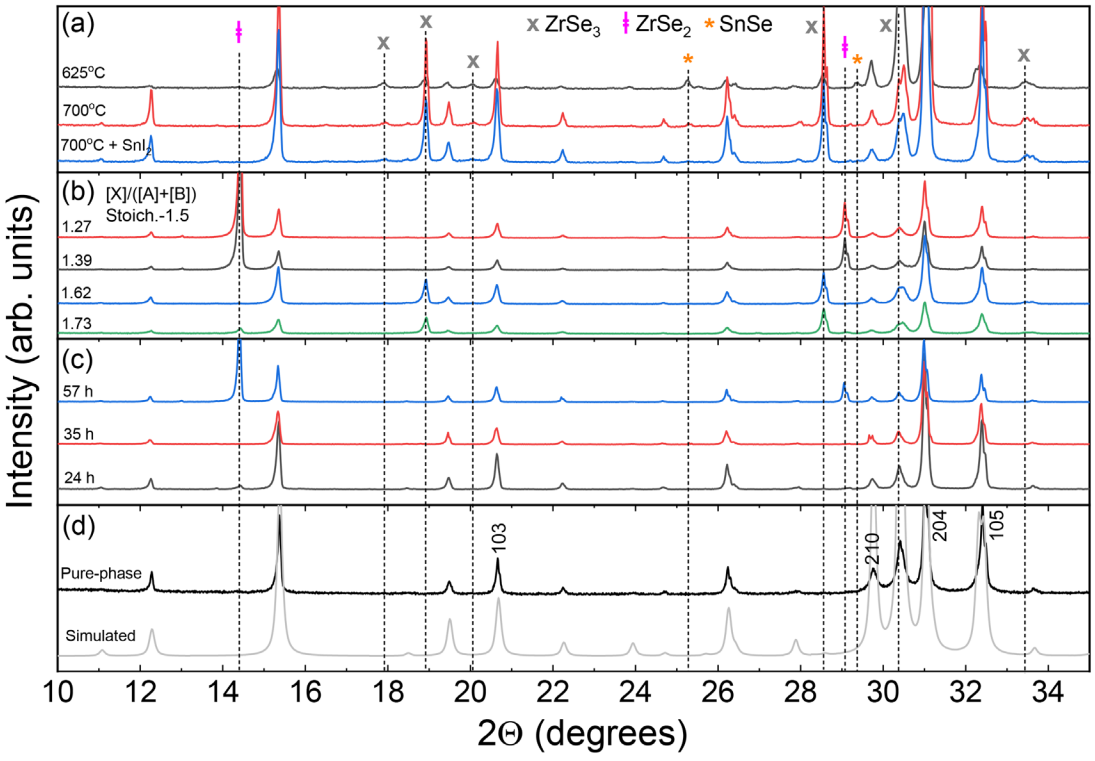

Figure 1. Phase composition analysis determined by X-ray diffraction method. (**a**) Diffractograms of $SnZrSe_3$ powder synthesized at various temperatures in a vertical position without and with transport agent. (**b**) Diffractograms of $SnZrSe_3$ powder samples synthesized in the same experiment at 740 °C temperature in a horizontal position with different initial Se-content in the precursor as indicated in the graph. (**c**) Diffractograms of $SnZrSe_3$ powder annealed for different durations. Top temperature – 700 °C, SnI_2 transport agent, position – horizontal, precursor composition - stoichiometric. (**d**) XRD pattern of collected and grinded crystals synthesized at 700 °C in horizontal position with a transport agent. Diffractogram of pure $SnZrSe_3$ phase was simulated using CIF file (*underlying data*[23]).

$SnZrSe_3$ powder phase purity. In the initial experiments we used long annealing durations to facilitate a complete solid-state reaction. However, we noticed that shorter annealing durations yielded lower concentration of secondary phases (Figure 1c). In the samples annealed under identical conditions but with different durations, we found that almost pure-phase powder was obtained annealing for 35 h instead of 60 h or more used previously (Figure 1c). Longer or shorter than 35 h annealing durations resulted in the formation of $ZrSe_2$ phase which concentration was much higher in the sample synthesized for a long period of time. This suggested that $SnZrSe_3$ formed relatively quickly and under prolonged annealing time slowly decomposed into binary phases. Therefore, from these results we can infer that 700 °C is close to the decomposition temperature of $SnZrSe_3$.

Based on the obtained results we propose a simplified reaction mechanism described below. During the temperature ramp in the synthesis process, it is suggested that SnSe is formed first, which crystallizes already at 300 °C[24]:

$$Sn(l) + \frac{1}{x} Se_x(g) \rightarrow SnSe(s) \quad (1)$$

where *l*, *g* and *s* indicate liquid, gaseous and solid states of matter; *x* denotes Se molecule size, which can be from 2 to 8 depending on the temperature[25]. In parallel, Zr reacts with Se vapour and $ZrSe_2$ is formed as the most stable form of Zr – Se system[26,27]:

$$Zr(s) + \frac{1}{x} Se_x(g) \rightarrow ZrSe_2(s) \quad (2)$$

Above 600 °C, SnSe enters a gaseous phase and starts to react with zirconium diselenide:

$$SnSe(g) + ZrSe_2(s) \rightarrow SnZrSe_3(s) \quad (3)$$

When there is a surplus of Se in the atmosphere, a competing reaction occurs:

$$ZrSe_2(s) + \frac{1}{x} Se_x(g) \rightarrow ZrSe_3(s) \quad (4)$$

Therefore, we believe that the thermodynamic balance between reactions (3) and (4) which depends on spatial separation of materials, partial Se pressure and annealing temperature determine the final product composition. While inspecting the ampoule annealed sequentially first at 700 °C and then at 800 °C, it was noticed that after the second annealing large $SnZrSe_3$ crystals deteriorated, and small fine needle-like crystals typical for $ZrSe_3$ were found (Figure S1 in *Extended data*[23]). This indicated that $SnZrSe_3$ decomposes at higher temperatures. This observation was in agreement with the results obtained from time-dependent annealing series, where prolonged synthesis duration at 700 °C led to decomposition of $SnZrSe_3$. Therefore, to synthesize $SnZrSe_3$ phase with high yield, it is essential to keep balance between top temperature and annealing duration. With our experimental setup it was around 35 h at 700 °C. However, if lower temperature is applied, longer duration may be required and vice versa.

In this study, to obtain a pure single-phase $SnZrSe_3$ powder, a part of large needle-shaped crystals was collected from the ampoule's walls and was grinded in a mortar. Other crystals were used as-grown for single crystal XRD, Raman scattering and electrical measurements. The XRD pattern of thus obtained powder is presented in Figure 1d. A very good match was found between the experimental XRD pattern and the one simulated from single crystal XRD data. No traces of secondary phases were detected. Note that intensity of XRD peaks of (h0l) planes was higher than in the simulated pattern (Figure 1d). This shows that a preferred orientation of (h0l) planes was present even in the powder sample because needle-like shaped grains tend to orient with their long axis parallel to the surface. Single-phase powder was later used for optical measurements.

Determination of the $SnZrSe_3$ structure

To determine the crystalline structure of $SnZrSe_3$, needle shaped crystal with dimensions of 0.25 × 0.02 × 0.015 mm and synthesized at 700 °C was selected for single crystal X-ray diffraction measurements. The summary of crystallographic information is presented in Table 1. More details on the refinement procedure and parameters can be found in the experimental description and crystallographic information file (*Underlying data*[23]) attached to the publication.

It was determined that $SnZrSe_3$ crystal is orthorhombic and belongs to space group *Pnma* (Figure 2a). The calculated unit cell parameters were a = 9.5862(4) Å, b = 3.84427(10) Å, c = 14.3959(5) Å and unit cell volume V = 530.52(3) $Å^3$. The needle axis of the crystal habit corresponded to the shortest crystallographic axis *b*. The X-ray structural analysis showed that the crystalline structure of $SnZrSe_3$ compound was isomorphous and isostructural to the sister compound $SnZrS_3$[28]. The fundamental building block of the crystalline structure was a ribbon (Figure 2b) which comprised of double edge-sharing Zr octahedra extending along *b* direction indefinitely. Within a ribbon and along *b* direction atoms are held by strong bonds as evidenced by the short interatomic distances of < 3 Å (Table 1). On the contrary, ribbons themselves are held together via van der Waals forces because of the longer interatomic distances (> 3 Å) found along directions *a* and *c* (Table 1). Within a unit cell cations occupy two non-equivalent sites Sn(1) and Zr(1), whereas anions have three distinct positions (Figure 2b). Sn(1) is coordinated with three Se atoms forming a trigonal pyramidal geometry, whereas Zr is coordinated with six Se atoms forming a distorted octahedra geometry. Additionally, the bonding environment around Sn cation in terms of bond length was found to be anisotropic (Figure 2c). Sn-Se bonds which are shorter than 3 Å are part of the ribbon structure, whereas in other directions they are longer than 3 Å giving a clear spatial separation between ribbons.

Optical characterisation of bandgap

For the optical characterization of $SnZrSe_3$, single-phase powder as determined from XRD measurements was selected. To examine if there were any impurity phases present on the surface of the powder, Raman scattering measurements were conducted. As seen before, XRD results showed no evidence of

Table 1. Summary of $SnZrSe_3$ single crystal crystallographic information. Crystallographic information was collected using single crystal XRD method and based on $SnZrSe_3$ crystal synthesised at 700 °C temperature. The key information was selected.

Compound	Crystal system	Space group	Unit cell parameters		
			a, Å	b, Å	c, Å
$SnZrSe_3$	Orthorhombic	*Pnma*	9.5862(4)	3.84427(10)	14.3959(5)
Atomic coordinates					
Atom	WP	x	y	x	U(eq)
Sn(1)	4c	4556(1)	7500	6664(1)	22(1)
Zr(1)	4c	1608(1)	2500	5498(1)	12(1)
Se(1)	4c	2697(1)	2500	7191(1)	16(1)
Se(2)	4c	3318(1)	7500	4876(1)	13(1)
Se(3)	4c	-155(1)	7500	6104(1)	11(1)
Geometric parameters					
Within ribbon (along *b*)		Intra ribbon (along *a*)		Inter ribbon (along *c*)	
Bond	Length, Å	Bond	Length, Å	Bond	Length, Å
Sn(1)-Se(1)	2.7291(5)	Se(2)-Se(2)	3.771	Sn(1)-Se(3)	3.225
Sn(1)-Se(2)	2.8352(7)	Sn(1)-Se(2)	3.573	Se(1)-Se(3)	3.736
Zr(1)-Se(1)	2.6514(7)				
Zr(1)-Se(2)	2.6798(5)				
Zr(1)-Se(3)	2.7041(5)				

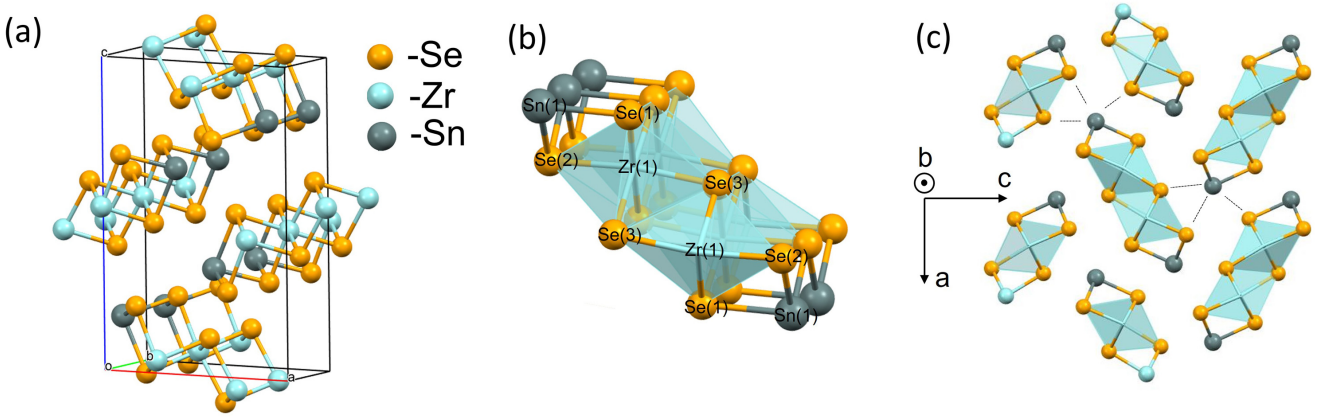

Figure 2. Crystalline structure of needle-like $SnZrSe_3$ phase. Single crystal XRD results confirmed that $SnZrSe_3$ crystal is orthorhombic (**a**) The main building block of $SnZrSe_3$ structure is ribbon which is presented in (**b**) with labelled atom sites. (**c**) The projection of $SnZrSe_3$ crystal structure on (*a, c*) plane highlight the anisotropy around Sn cation. Dashed lines indicate > 3 Å interatomic distances in Sn coordination environment.

secondary phases (Figure 1c). For the Raman scattering study, additional samples were measured – a $SnZrSe_3$ monocrystal which served as a reference case. Raman spectra contained vibrational bands located at 71, 119, 133, 160, 196 and 243 cm^{-1} (Figure 3a). Because there is no reference Raman spectrum of $SnZrSe_3$ in the literature, we first examined if there were secondary phases that had been observed in XRD patterns. Positions of the main and the most intensive Raman bands of $ZrSe_2$[29], SnSe[30] and $ZrSe_3$[31] are shown as dotted lines (Figure 3a). No evidence of $ZrSe_3$ phase was found. However, one Raman band of SnSe (71 cm^{-1}) and three bands of $ZrSe_2$ (134 cm^{-1}, 196 cm^{-1}, 242 cm^{-1}) overlap very well with some of the $SnZrSe_3$ bands. Despite a good match, we believe it is not a response from secondary phases, but because of structural similarities between $SnZrSe_3$ and $ZrSe_2$ (SnSe) that give rise to similar vibrational bands. The main structural element in $ZrSe_2$ is ZrX_6 octahedral which is also the case in $SnZrSe_3$ (Figure 2b). Coordination environment of Sn in SnSe and $SnZrSe_3$ also share similar structural features therefore rendering alike Raman bands. In addition, the Raman spectrum of $SnZrSe_3$ monocrystal perfectly matched with Raman spectrum of the $SnZrSe_3$ powder sample. This strongly supports that $SnZrSe_3$ powder was free of secondary phases and overlapping bands were a result of similar structural characteristics between $SnZrSe_3$ and $ZrSe_2$ (SnSe).

To estimate the absorption and to calculate optical bandgap and other critical points in the electronic band, diffuse reflectance was measured of the single-phase powder sample (Figure 3b). According to the Schuster-Kubelka-Munk formulation, apparent absorption and diffuse reflection are related as follows[32]:

$$F(R_\infty) = \frac{(1-R_\infty)^2}{2R_\infty} = \frac{K}{S} \quad (5)$$

Where, R_∞ - diffuse reflectance, K – apparent absorption, S – reflection coefficient.

Assuming S did not change considerably over the measured energy range, $F(R_\infty)$ was taken to reflect the $SnZrSe_3$ absorption coefficient. Diffused reflectance together with the calculated $F(R_\infty)$ are depicted in Figure 3b. To estimate the bandgap, we first applied the common Tauc method[33]. In brief, material's absorption coefficient (for photon energy above the bandgap) is proportional to the material's bandgap as follows: $\alpha E_{ph} \approx C(E_{ph}-E_g)^n$, where α is absorption coefficient, C – constant reflecting joint density of states in the bands, E_{ph} – is a photon energy, E_g – material's bandgap and n -exponent depending on the optical transition nature: for direct transition n=2, for indirect n=0.5. Then, to find the bandgap value, $(\alpha E_{ph})^n$ is plotted versus E_{ph} and fitted linearly. A linear fitting region is extrapolated until it crosses x axis where α≈0 and the crossing point is defined as material's bandgap. Direct transition was considered for $SnZrSe_3$ therefore $(F(R_\infty)\cdot E)^2$ vs E plot was used (Figure 3b, inset). The fitted linear region near the absorption edge resulted in a bandgap value of around 1.16 eV. In the second approach, to estimate the position of critical points (CP) in the band structure, the second derivative of $F(R_\infty)$ was calculated (Figure 3c). To reduce background noise and highlight CP features, data points were smoothed using Savitzky-Golay methods with 3rd order polynomial and a 100 point window. Note, that we did not fit the derivative with the Aspnes' function, because to obtain correct fitting results, high-accuracy measurements of material dielectric function are required. Nevertheless, the position of CP can be still estimated as the inflexion point of the CP feature, which typically has one positive and one negative extrema (Figure 3c, indicated by arrows). In addition, to validate the certainty of CPs identified in the spectrum, we calculated second derivative under various smoothing conditions for the same sample and measured the diffuse reflectance on $SnZrSe_3$ sample made from another batch. In all cases, inflexion points were located at the same positions (Figure S2 in *Extended data*[23]). First, clear CP features below the $SnZrSe_3$ absorption edge were observed at 0.65 and 0.87 eV, respectively. The position of these CPs was in very close agreement with H_2O absorption bands which are located at 1940 nm (~0.64 eV) and 1450 nm (~0.85 eV)[34]. This indicated that H_2O was present in $BaSO_4$ which was used as a white reference plate in the diffuse reflectance measurements. Such a case is quite common when $BaSO_4$ is used as a reference

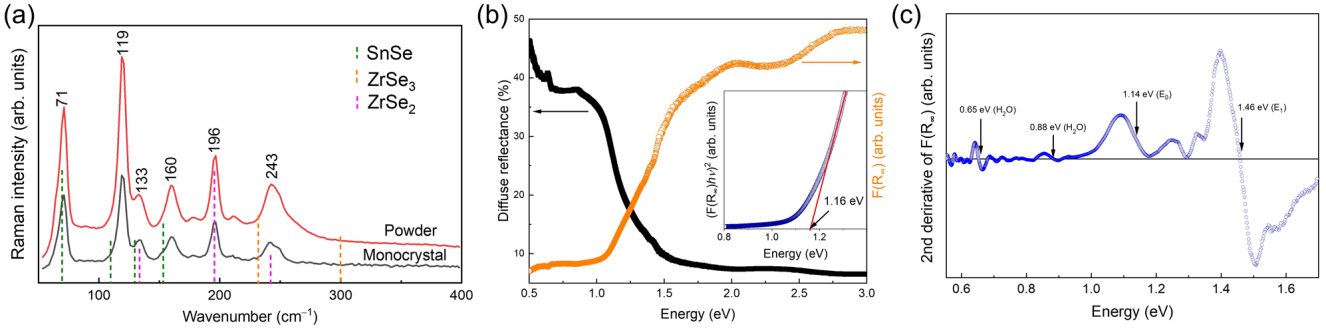

Figure 3. Raman spectra and optical properties of $SnZrSe_3$ powder. (**a**) Raman scattering spectra of single phase $SnZrSe_3$ powder and monocrystal synthesized at 700°C. Excitation wavelength - 532 nm. (**b**) Diffuse reflectance spectrum and thereof calculated apparent absorption using eq. 5 of single-phase $SnZrSe_3$ powder. Inset – Tauc plot of $SnZrSe_3$ around absorption edge. (**c**) Second derivative of measured apparent absorption as a function of energy of single-phase $SnZrSe_3$ powder.

plate. Other CPs were located at 1.14 and 1.46 eV (Figure 3c). The low energy CP was assigned to the $SnZrSe_3$ bandgap because it coincided well with the value estimated from the Tauc plot (Figure 3b). However, all other higher energy CPs cannot be assigned to a specific optical transition and is beyond the scope of this work. Based on the diffuse reflectance results, $SnZrSe_3$ bandgap was around 1.15 eV which is almost twice as large as predicted from first-principles[19] and is substantially higher than measured by Richard[20]. First-principles calculations using hybrid potentials can predict bandgaps consistent with experimental values therefore such large discrepancy we relate to one of the two reasons: (i) $SnZrSe_3$ is an indirect bandgap semiconductor and using diffuse reflectance method we were not able to clearly detect weak indirect optical transitions which would be expected to be lower in energy than direct (ii) due to low density of states at the band edges, strong optical absorption starts with an high onset leading significant absorption only at higher photon energies[19]. The value measured by Richard was very close to the water absorption band located at 1450 nm. Although we consistently found a bandgap value of about 1.15 eV, more samples such as thin films, and other bandgap measurement methods would be useful to consolidate the real bandgap value of $SnZrSe_3$ and nature of transition (direct/indirect).

Electrical properties

Conductivity type is a very important factor when considering the formation of semiconductor heterojunctions. Without intentional doping, conductivity usually depends on the dominating intrinsic point defects in the material, which in turn are related to the compound stoichiometry. To study conductivity properties of $SnZrSe_3$, we first tested the largest needle-like crystals with a hot-point-probe method. This method allows us to identify the conductivity type by observing current/voltage sign upon increase in temperature gradient between probes. Before measurements, the system was calibrated with well-known *n*-type commercial fluorine doped SnO_2 (SigmaAldrich) sample and boron doped commercial *p*-type (100) Si wafer. It turned out that some as-grown crystals showed a constant positive voltage change upon temperature gradient increase and some – negative (Figure 4a). This indicated that $SnZrSe_3$ can exhibit both *n* and *p*-type conductivity. Note that *n*-type behaviour was much more pronounced suggesting higher carrier concentration was present in *n*-type than in *p*-type crystals or much higher mobility of electrons. This was also in-line with calculated resistivity which was two orders of magnitude higher for *p*-type sample (Table 2). To find if there was a relation between off-stoichiometry and conductivity type, we measured the chemical composition of crystals showing

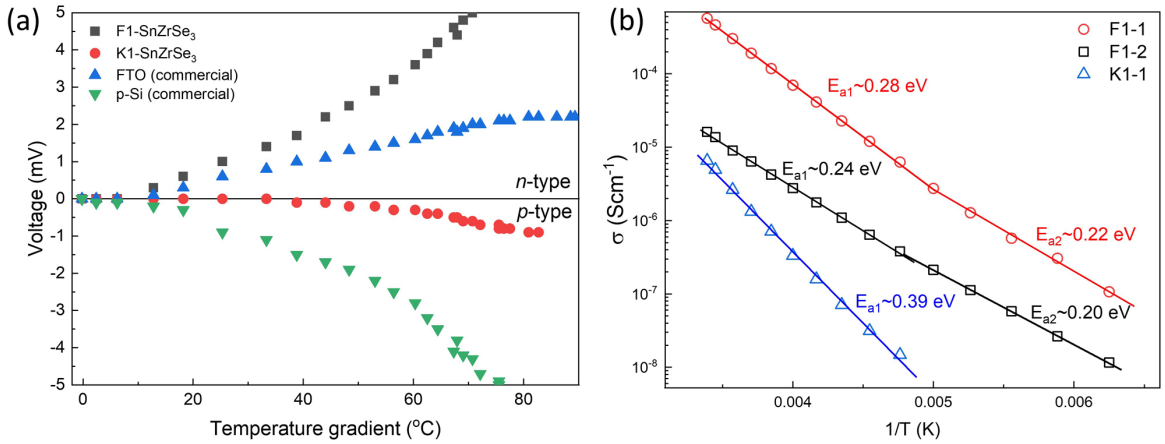

Figure 4. Electrical properties of $SnZrSe_3$ crystals. (**a**) Voltage as a function of a temperature difference between probes measured on $SnZrSe_3$ crystals using hot-point-probe method. Commercial FTO (fluorine doped SnO_2) and boron doped Si wafer were used to calibrated system. (**b**) Electrical conductivity as a function of reciprocal temperature in three single-crystal $SnZrSe_3$ samples.

Table 2. Chemical composition and electrical parameters of $SnZrSe_3$ crystals from F1 and K1 batches. Two batches (F1 and K1) of crystals were studied which showed pronounced *n*- and *p*-type conductivity behaviour. Chemical composition clearly showed correlation with composition in uniform crystal samples.

Sample	Sn, at.%	Zr, at.%	Se, at.%	Sn/Zr	Se/(Sn+Zr)	ρ_s, Ω·cm	E_{a1}, eV	E_{a2}, eV
n-F1 (HHP)	21.5±1.1	20.9±0.4	57.6±1.3	1.03	1.36			
p-K1 (HHP)	22.1±1.5	21.4±0.9	56.5±1.0	1.03	1.30			
F1-1	22.0±0.12	21.0±0.13	57.0±0.13	1.05	1.33	$1.5 \cdot 10^3$	0.28	0.22
F1-2	21.0±0.52	21.5±0.12	57.5±0.41	0.98	1.35	$3.9 \cdot 10^4$	0.24	0.20
K1-1	19.4±0.09	22.4±0.2	58.2±0.14	0.86	1.39	$1.7 \cdot 10^5$	0.39	-

n and *p*-type behaviour, respectively. The average composition of the crystals measured over more than 5 points are summarized in Table 2. In both samples, the cationic ratio A/B was identical, whereas the *n*-type crystal was slightly more Se-rich than p-type, but both were Se-deficient with respect to stoichiometric ratio of [X]/([A]+[B]) which is 1.5. At this point, it is difficult to confirm if the different Se quantity was the origin of respective conductivity type and would require more samples to be synthesized and tested. In addition, there was quite a large compositional variation as seen from the high standard deviation. Important to note that since iodine was used as a transport agent to facilitate the solid state reaction during synthesis, it could be inadvertently introduced in the lattice giving rise to extrinsic doping. Iodine could not be detected by EDX, but we acknowledge that very small amounts (beyond the EDX detection limit) can have a significant contribution to the conductivity behaviour. In summary, although the origin of doping is not clear in $SnZrSe_3$, the bipolar conductivity behaviour is a very desirable feature for semiconductor-based technologies[35].

To estimate the ionization potential (E_a) of defects contributing to the conductivity, temperature dependent *I-V* curves were measured. To avoid grain boundary effects, as monolithic as possible $SnZrSe_3$ samples were selected (Figure S3 in *Extended data*[23]). However, due to their small size, their conductivity type could not be measured directly by HPP and was assumed from the measurements of larger crystals from the same batch. We found that the resistivity of samples varied in 10^3 – 10^5 Ω·cm range highlighting the insulating nature of $SnZrSe_3$. Calculated E_a of defects are summarized in Table 2 and Figure 4b. We see that for F1 series samples two E_a were calculated, but because conductivity is the product of carrier concentration and carrier mobility, it cannot be ruled out that reduction in E_a was because of the change of carrier scattering mechanisms, and therefore increased mobility upon temperature decrease. Overall, all defects that were found to contribute to the conductivity can be considered as deep defects, because E_a » 0.025 eV, which is a thermal excitation energy at room temperature (kT), k is Boltzmann constant and T – temperature (295 K). Chemical composition of the crystals was also measured (Table 2) to link composition with conductivity behaviour. These crystals were much more homogenous as evidenced by a small standard deviation. Notably, the specific resistance was found to correlate with the Sn/Zr ratio: the more Sn-rich sample was, the smaller resistivity. In addition, it is likely that Sn-rich composition also led to *n*-type conductivity, whereas Sn-deficiency – to the *p*-type. This would also explain why in the Sn-deficient sample (K1-1) we observed very different E_a than in the other two cases. E_a in F1 samples was related to the donor defects, whereas in K1 – to the acceptor type defects. This was not obvious when the composition of large crystals was measured because of their chemical inhomogeneity. Resistivity can also be related to the gradual change of Se content as well. However, to rely on the Se ratio to the cations is less accurate, because we found small amounts of oxygen present in the crystals, especially if exposed for a long time in the ambient environment. The oxygen is most likely adsorbed from the air or in some amorphous state because phase composition determined by XRD of the powder sample that was stored for more than half a year under ambient conditions (T=20-25°C, RH=30-60%) did not change (Figure S4 in *Extended data*[23]). This also shows high thermodynamic stability of the $SnZrSe_3$.

Discussion

A characteristic structural feature of perovskite compounds is that cation B forms an octahedra geometry with sharing corners[36]. In fact, the stability of perovskite structures are predicted by estimating Goldschmidt's tolerance factor, *t*, which reflects an ability to squeeze octahedra in a cubic sub-lattice[37]. However, ABX_3 chalcogenides do not follow predictions based on *t* only. None of the ABX_3 chalcogenides exist in a perfect cubic structure even when *t*=1.0 (which is a golden ratio for cubic perovskite). Because chalcogen ionic radius is much larger than that of oxygen, the octahedral factor (μ) must also be accounted for. Then, *t* is plotted against μ, it can be clearly seen that only a few ABX_3 chalcogenides fall in the region of having a perovskite structure[17]. For $SnZrSe_3$ calculated *t* and μ values are 0.79 and 0.36, which falls outside the perovskite region ($t > 0.85$, $\mu > 0.4$).

Instead, ABX_3 chalcogenides are found to exist in distorted perovskite (model structure – $GdFeO_3$), needle-like (model structure NH_4CdCl_3) and hexagonal (model structure $BaNiO_3$) structures. Other crystal structures also exist in ABX_3 chalcogenides, for example, $CeTmS_3$-type in $A^{3+}B^{3+}X^{2-}{}_3$[38], $CuTaS_3$-type in $A^{1+}B^{5+}X^{2-}{}_3$[39] and there are other possible variations although more rare. In needle-like and hexagonal structures, B cation octahedra is sharing edges (faces) instead of corners as is the case in $SnZrSe_3$ (Figure 2c). This will give rise to anisotropic carrier transport because low effective mass is expected in the direction of edge-sharing octahedra compared to other directions. Indeed, high anisotropy in electronic band dispersion was shown in $SnZrS_3$ and $SnZrSe_3$ (needle-like phase) using the first-principles calculations[19].

Additionally, it is important to note the difference in bonding environment between $SnZrSe_3$ and other needle-like ABX_3 chalcogenides containing alkali or alkaline earth cations, for instance, $SrZrSe_3$ or $RbCdCl_3$. In $SrZrSe_3$, cation A is positioned almost equidistantly from the nearest neighbouring atoms[40], whereas in $SnZrSe_3$ as shown before there is a clear anisotropy in terms of interatomic distances (Figure 2c). The origin of the ribbon-like structure in $SnZrSe_3$ could be related to the stereochemically active lone electron pair. On theoretical grounds, it has been shown that stereochemically active lone pairs lead to distorted low symmetry crystal structures[41]. Sn in $SnZrSe_3$ is in a +2 valence state which leads to two unpaired 5s electrons. For the binary compounds, if there is a strong interaction between cation s states and anion p states, electronic stabilization is achieved through lattice distortion and lone electron pair is ejected outwards forming a structural void. That leads to asymmetric bonding around lone electron pair containing cation. Many chalcogenides containing cation with lone electron pair such as Sb_2Se_3, Sb_2S_3, Bi_2S_3, $SnHfS_3$, $SnZrS_3$, $PbHfS_3$ and $PbZrS_3$ have a ribbon-like low symmetry

crystal structure. Because of these structural similarities at least binary compounds also share some electronic and optical characteristics, for instance indirect bandgap with a small difference between direct and indirect gaps and anisotropic carrier transport properties[42]. Based on first-principles calculations, $SnZrSe_3$ is predicted to have a small (< 0.1 eV) difference between indirect and direct gaps as well[19]. Such characteristic is highly desired in absorber materials for photovoltaics because high absorption coefficient and long carrier lifetime can be realised simultaneously[42]. On one hand absorption coefficient (α) depends on the density of states in the bands. If states at direct gap are dispersive it can lead to slowly increasing α resulting in significant absorption onset. Based on optical properties calculated for $SnZrSe_3$, $\alpha > 10^4$ cm^{-1} is reached for photon energy > 1.5 eV which renders an onset of around 0.9 eV[19]. Another theoretical work also shows that among ABX_3 chalcogenides those in needle-like phase have a larger absorption onset than those in perovskite structure[12], and this was measured for $SrZrS_3$ case experimentally[43]. On the hand, in materials with dispersive bands, a high carrier mobility can be expected. Consequently, for practical application, for instance solar cells, an optimum absorber thickness will be required to balance between charge carrier mobility, lifetime and absorption coefficient.

In this work, we found that $SnZrSe_3$ showed *p* as well as *n* type conductivity behaviour. Ambipolar behaviour was also recently realised in $BaZrS_3$ thin films[44]. This is in contrast to other multicomponent well-known Cu-based photovoltaic materials such as $Cu(In,Ga)Se_2$, $Cu_2ZnSn(Se,S)_4$, $CuSb(Se,S)_2$ and $Cu_2Sn(Se,S)_3$ where usually one type carrier is dominant. Because of low formation energy of Cu vacancy defect (acceptor type), these materials are intrinsically p-type[45–48]. Inability to alter the conductivity type and magnitude on demand, puts constrains on the device structure and requires formation of heterojunctions. On the contrary, if a semiconductor can be tuned to behave as *p* or *n* type, it opens up wider possibilities to design device structure, for example employing homojunctions and there is also a wider choice of partner layers for formation of heterojunctions. Bipolar dopability is therefore desired in the material because it facilitates the optimisation of device design for targeted application.

$SnZrSe_3$ is a promising material candidate for photovoltaic application. Nonetheless, to really highlight the potential of this material, the deposition of $SnZrSe_3$ in thin film form should be demonstrated and absolute values of optical absorption measured. This has not been done or reported thus far. Based on the experience in synthesis of other ABX_3 chalcogenide thin films ($BaZrS_3$)[16], deposition process of $SnZrSe_3$ could be challenging. Because of the large difference in vapour pressure of constituting elements, conventional chalcogenide thin film synthesis methods can be unsuitable. Therefore, likely alternative synthesis approaches should be explored to synthesize $SnZrSe_3$ thin films.

Conclusions

In this work, we studied the properties of $SnZrSe_3$ intending to explore ABX_3 chalcogenide materials beyond the perovskite structure. We confirmed that the ground phase of $SnZrSe_3$ is needle-like (s.g. *Pnma*) where the main building block was a ribbon forming a quasi-one-dimensional crystal structure. Coordination anisotropy around cation A was observed in $SnZrSe_3$ which was a sign of a stereochemically active electron lone pair of Sn. The bandgap of $SnZrSe_3$ was found to be 1.15 eV which is much smaller than in perovskite chalcogenides, therefore, broadening application range of ABX_3 chalcogenides. In addition, we found that as-grown $SnZrSe_3$ crystals were insulating (ρ_s = 10^3-10^5 Ω·cm), showed bipolar dopability and deep intrinsic defects. In terms of ribbon-like crystal structure and optical bandgap, $SnZrSe_3$ has similar properties as Sb_2X_3 – which is one of the most perspective materials for earth-abundant and non-toxic photovoltaics, but $SnZrSe_3$ offers a wider range of tunability in terms of doping and bandgap. However, the next important step in the validation of $SnZrSe_3$ prospects is to find a synthesis approach for thin film deposition, which could be not as straightforward as evidenced from experience with perovskite chalcogenides.

Ethics and consent

Ethical approval and consent were not required.

Data availability

Underlying data

Zenodo: Dataset for publication "Synthesis and physical characteristics of narrow bandgap chalcogenide SnZrSe3". https://doi.org/10.5281/zenodo.7867349[23].

This project contains the following underlying data:

- Sample description.txt (synthesis conditions of the samples presented in the publication).
- F1IS_V_6244.cif (crystallographic information file about $SnZrSe_3$ structure as determined by single-crystal XRD method; CIF can be opened with free of charge available software, e.g. VESTA (https://jp-minerals.org/vesta/en/), Mercury (https://www.ccdc.cam.ac.uk/solutions/csd-core/components/mercury/)).
- XRD.zip (raw XRD patterns of powder samples presented in the publication in .ras and .raw formats; ras file can be read and plotted using open-source platform Labplot; raw/ras files can be opened and analysed in Profex (free of charge, https://www.profex-xrd.org/)).
- Raman.zip (raw Raman spectra in .txt format and OriginPro project file where data was plotted; alternatively, Raman spectra can also be read and plotted using open-source platform Labplot (https://labplot.kde.org/)).

– Optics.zip (raw diffuse reflectance data in .txt format and OriginPro project file where data was processed and plotted; diffuse reflectance spectra can also be read, analysed and plotted using open-source platform Labplot (https://labplot.kde.org/)).

– JV-T.zip (I-V curves at specific temperature in .txt format and OriginPro project files where data was processed and plotted; I-V data files can be read, analysed and plotted using open-source platform Labplot (https://labplot.kde.org/)).

– Images.zip (optical photographs of the sample and untreated SEM images of crystals).

CIF files were deposited with the Cambridge Crystallographic Data Centre CCDC/ICSD, deposition number CSD 2166561, and can be accessed upon request (https://www.ccdc.cam.ac.uk/structures/).

Extended data

Zenodo: Dataset for publication "Synthesis and physical characteristics of narrow bandgap chalcogenide SnZrSe3". https://doi.org/10.5281/zenodo.7867349[23].

This project contains the following extended data:

– Extended data.pdf (additional information supporting claims in the publication with direct link to the main text, such as figures).

Data are available under the terms of the Creative Commons Attribution 4.0 International license (CC-BY 4.0).

References

1. Van Le Q, Jang HW, Kim SY: **Recent advances toward high-efficiency halide perovskite light-emitting diodes: review and perspective.** *Small Methods.* 2018; **2**(10): 1700419.
Publisher Full Text
2. Wu H, Ge Y, Niu G, *et al.*: **Metal halide perovskites for X-ray detection and imaging.** *Matter.* 2021; **4**(1): 144–163.
Publisher Full Text
3. Jena AK, Kulkarni A, Miyasaka T: **Halide Perovskite Photovoltaics: Background, Status, and Future Prospects.** *Chem Rev.* 2019; **119**(5): 3036–3103.
PubMed Abstract | Publisher Full Text
4. Ciccioli A, Latini A: **Thermodynamics and the Intrinsic Stability of Lead Halide Perovskites $CH_3NH_3PbX_3$.** *J Phys Chem Lett.* 2018; **9**(13): 3756–3765.
PubMed Abstract | Publisher Full Text
5. Ke W, Kanatzidis MG: **Prospects for low-toxicity lead-free perovskite solar cells.** *Nat Commun.* 2019; **10**(1): 965.
PubMed Abstract | Publisher Full Text | Free Full Text
6. Huang YT, Kavanagh SR, Scanlon DO, *et al.*: **Perovskite-inspired materials for photovoltaics and beyond-from design to devices.** *Nanotechnology.* 2021; **32**(13): 132004.
PubMed Abstract | Publisher Full Text
7. Kiermasch D, Rieder P, Tvingstedt K, *et al.*: **Improved charge carrier lifetime in planar perovskite solar cells by bromine doping.** *Sci Rep.* 2016; **6**: 39333.
PubMed Abstract | Publisher Full Text | Free Full Text
8. Zakutayev A, Caskey CM, Fioretti AN, *et al.*: **Defect Tolerant Semiconductors for Solar Energy Conversion.** *J Phys Chem Lett.* 2014; **5**(7): 1117–1125.
PubMed Abstract | Publisher Full Text
9. Huang H, Bodnarchuk MI, Kershaw SV, *et al.*: **Lead Halide Perovskite Nanocrystals in the Research Spotlight: Stability and Defect Tolerance.** *ACS Energy Lett.* 2017; **2**(9): 2071–2083.
PubMed Abstract | Publisher Full Text | Free Full Text
10. Brandt RE, Poindexter JR, Gorai P, *et al.*: **Searching for "defect-tolerant" photovoltaic materials: combined theoretical and experimental screening.** *Chem Mater.* 2017; **29**(11): 4667–4674.
Publisher Full Text
11. Swarnkar A, Mir WJ, Chakraborty R, *et al.*: **Are chalcogenide perovskites an emerging class of semiconductors for optoelectronic properties and solar cell?** *Chem Mater.* 2019; **31**(3): 565–575.
Publisher Full Text
12. Sun YY, Agiorgousis ML, Zhang P, *et al.*: **Chalcogenide perovskites for photovoltaics.** *Nano Lett.* 2015; **15**(1): 581–585.
PubMed Abstract | Publisher Full Text
13. Niu S, Zhao B, Ye K, *et al.*: **Crystal growth and structural analysis of perovskite chalcogenide $BaZrS_3$ and Ruddlesden–Popper phase $Ba_3Zr_2S_7$.** *J Mater Res.* 2019; **34**: 3819–3826.
Publisher Full Text
14. Wei X, Hui H, Zhao C, *et al.*: **Realization of $BaZrS_3$ chalcogenide perovskite thin films for optoelectronics.** *Nano Energy.* 2020; **68**: 104317.
Publisher Full Text
15. Wei X, Hui H, Perera S, *et al.*: **Ti-Alloying of $BaZrS_3$ Chalcogenide Perovskite for Photovoltaics.** *ACS Omega.* 2020; **5**(30): 18579–18583.
PubMed Abstract | Publisher Full Text | Free Full Text
16. Márquez JA, Rusu M, Hempel H, *et al.*: **$BaZrS_3$ Chalcogenide Perovskite Thin Films by H_2S Sulfurization of Oxide Precursors.** *J Phys Chem Lett.* 2021; **12**(8): 2148–2153.
PubMed Abstract | Publisher Full Text
17. Sopiha KV, Comparotto C, Márquez JA, *et al.*: **Chalcogenide Perovskites: Tantalizing Prospects, Challenging Materials.** *Adv Opt Mater.* 2022; **10**(3): 2101704.
Publisher Full Text
18. Moroz NA, Bauer C, Williams L, *et al.*: **Insights on the Synthesis, Crystal and Electronic Structures, and Optical and Thermoelectric Properties of $Sr_{1-x}Sb_xHfSe_3$ Orthorhombic Perovskite.** *Inorg Chem.* 2018; **57**(12): 7402–7411.
PubMed Abstract | Publisher Full Text
19. Bellil NB, Litimein F, Khachai H, *et al.*: **Structural, optoelectronic and thermodynamic characteristic of orthorhombic $SnZrCH_3$(CH=S, Se) compounds: Insights from DFT computations.** *Mater Today Commun.* 2021; **27**: 102427.
Publisher Full Text
20. Richard AP: **Single crystal growth, powder synthesis and characterization of layered chalcogenide semiconductors.** Oregon State University, 2011.
Reference Source
21. Sheldrick GM: **A short history of *SHELX*.** *Acta Crystallogr A.* 2008; **64**(Pt 1): 112–122.
PubMed Abstract | Publisher Full Text
22. Sheldrick GM: **Crystal structure refinement with *SHELXL*.** *Acta Crystallogr C Struct Chem.* 2015; **71**(Pt 1): 3–8.
PubMed Abstract | Publisher Full Text | Free Full Text
23. Kondrotas R, Juskenas R, Krotkus A, *et al.*: **Dataset for publication "Synthesis and physical characteristics of narrow bandgap chalcogenide $SnZrSe_3$".** *Zenodo.* 2022.
http://www.doi.org/10.5281/zenodo.7867349
24. Pallavolu MR, Minnam Reddy VR, Guddeti PR, *et al.*: **Development of SnSe thin films through selenization of sputtered Sn-metal films.** *J Mater Sci-Mater El.* 2019; **30**: 15980–15988.
Publisher Full Text
25. Rau H: **Vapour composition and critical constants of selenium.** *J Chem Thermodyn.* 1974; **6**(6): 525–535.
Publisher Full Text
26. Jain A, Ong SP, Hautier G, *et al.*: **Commentary: The Materials Project: A materials genome approach to accelerating materials innovation.** *APL Mater.* 2013; **1**(1): 011002.
Publisher Full Text

27. Ong SP, Wang L, Kang B, *et al.*: **Li-Fe-P-O2 Phase Diagram from First Principles Calculations.** *Chem Mater.* 2008; **20**: 1798–1807.
Publisher Full Text

28. Meetsma A, Wiegers G, De Boer J: **Structure determination of SnZrS3.** *Acta Cryst C.* 1993; **49**: 2060–2062.
Publisher Full Text

29. Mañas-Valero S, García-López V, Cantarero A, *et al.*: **Raman Spectra of ZrS_2 and $ZrSe_2$ from Bulk to Atomically Thin Layers.** *Appl Sci.* 2016; **6**(9): 264.
Publisher Full Text

30. Liu F, Parajuli P, Rao R, *et al.*: **Phonon anharmonicity in single-crystalline SnSe.** *Phys Rev B.* 2018; **98**(22): 224309.
Publisher Full Text

31. Zwick A, Renucci M, Kjekshus A: **Raman scattering in the IVB transition-metal trichalcogenides: ZrS_3, $ZrSe_3$, $ZrTe_3$ and $HfSe_3$.** *J Phys C Solid State.* 1980; **13**: 5603.
Publisher Full Text

32. Kubelka P: **Ein Beitrag zur Optik der Farbanstriche (Contribution to the optic of paint).** *Z Tech Phys.* 1931; **12**: 593–601.
Reference Source

33. Tauc J, Grigorovici R, Vancu A: **Optical properties and electronic structure of amorphous germanium.** *Physica Status Solidi (b).* 1966; **15**(2): 627–637.
Publisher Full Text

34. Curcio JA, Petty CC: **The near infrared absorption spectrum of liquid water.** *JOSA.* 1951; **41**(5): 302–304.
Publisher Full Text

35. Wei SH: **Overcoming the doping bottleneck in semiconductors.** *Comp Mater Sci.* 2004; **30**(3–4): 337–348.
Publisher Full Text

36. Young J, Rondinelli JM: **Octahedral rotation preferences in perovskite iodides and bromides.** *J Phys Chem Lett.* 2016; **7**(5): 918–922.
PubMed Abstract | Publisher Full Text

37. Goldschmidt VM: **Die gesetze der krystallochemie.** *Naturwissenschaften.* 1926; **14**: 477–485.
Publisher Full Text

38. Kuhar K, Crovetto A, Pandey M, *et al.*: **Sulfide perovskites for solar energy conversion applications: computational screening and synthesis of the selected compound $LaYS_3$.** *Energy Environ Sci.* 2017; **10**(12): 2579–2593.
Publisher Full Text

39. Sunshine SA, Ibers JA: **Redetermination of the structures of $CuTaS_3$ and Nb_2Se_9.** *Acta Crystallogr Sect C.* 1987; **43**: 1019–1022.
Publisher Full Text

40. Tranchitella LJ, Chen BH, Fettinger JC, *et al.*: **Structural Evolutions in the $Sr_{1-x}Ba_xZrSe_3$Series.** *J Solid State Chem.* 1997; **130**(1): 20–27.
Publisher Full Text

41. Walsh A, Payne DJ, Egdell RG, *et al.*: **Stereochemistry of post-transition metal oxides: revision of the classical lone pair model.** *Chem Soc Rev.* 2011; **40**(9): 4455–4463.
PubMed Abstract | Publisher Full Text

42. Kondrotas R, Chen C, Liu XX, *et al.*: **Low-dimensional materials for photovoltaic application.** *J Semicond.* 2021; **42**(3): 031701.
Publisher Full Text

43. Niu S, Huyan H, Liu Y, *et al.*: **Bandgap Control via Structural and Chemical Tuning of Transition Metal Perovskite Chalcogenides.** *Adv Mater.* 2017; **29**(9): 1604733.
PubMed Abstract | Publisher Full Text

44. Yu Z, Wei X, Zheng Y, *et al.*: **Chalcogenide perovskite $BaZrS_3$ thin-film electronic and optoelectronic devices by low temperature processing.** *Nano Energy.* 2021; **85**: 105959.
Publisher Full Text

45. Schroeder DJ, Hernandez JL, Berry GD, *et al.*: **Hole transport and doping states in epitaxial $CuIn_{1-x}Ga_xSe_2$.** *J Appl Phys.* 1998; **83**(3): 1519–1526.
Publisher Full Text

46. Li S, Lloyd MA, McCandless BE, *et al.*: **Effects of cation composition on carrier dynamics and photovoltaic performance in $Cu_2ZnSnSe_4$ monocrystal solar cells.** *Sol Energy Mater Sol Cells.* 2020; **205**: 110255.
Publisher Full Text

47. Welch AW, Zawadzki PP, Lany S, *et al.*: **Self-regulated growth and tunable properties of $CuSbS_2$ solar absorbers.** *Sol Energy Mater Sol Cells.* 2015; **132**: 499–506.
Publisher Full Text

48. Baranowski LL, Zawadzki P, Christensen S, *et al.*: **Control of doping in Cu_2SnS_3 through defects and alloying.** *Chem Mater.* 2014; **26**(17): 4951–4959.
Publisher Full Text

Open Peer Review

Current Peer Review Status: ✔ ✔

Version 2

Reviewer Report 01 June 2023

https://doi.org/10.21956/openreseurope.17286.r31734

© **2023 Zeng H.** This is an open access peer review report distributed under the terms of the Creative Commons Attribution License, which permits unrestricted use, distribution, and reproduction in any medium, provided the original work is properly cited.

✔ **Hao Zeng**
Department of Physics, University at Buffalo, Buffalo, NY, USA

I am satisfied with the revised version. The manuscript is ready for indexing.

Competing Interests: No competing interests were disclosed.

Reviewer Expertise: Chalcogenide perovskites, optoelectronic properties.

I confirm that I have read this submission and believe that I have an appropriate level of expertise to confirm that it is of an acceptable scientific standard.

Version 1

Reviewer Report 22 March 2023

https://doi.org/10.21956/openreseurope.16407.r31017

© **2023 Sun Y.** This is an open access peer review report distributed under the terms of the Creative Commons Attribution License, which permits unrestricted use, distribution, and reproduction in any medium, provided the original work is properly cited.

✔ **Yi-Yang Sun**
State Key Laboratory of High Performance Ceramics and Superfine Microstructure, Shanghai Institute of Ceramics, Chinese Academy of Science, Shanghai, China

It is enjoyable to read through this paper, which reports the synthesis and characterization of the compound $SnZrSe_3$, an unknown material so far. Even though $SnZrSe_3$ appears to be isostrutural to $SnZrS_3$, it is an important addition to the database of inorganic crystals. The description on the

experimental details and the discussion on the results are detailed and objective enough to assure the reader what has been done and what still requires further study. I have no reservation regarding the indedxing of this work. Nevertheless, given the complete open nature of this journal, I would like to add a discussion which might be of interest to the readers of this paper.

The "perovskite" structure, without any generalization, should be composed of corner-shared octahedra. In this sense, the ribbon-like structure of $SnZrSe_3$ with edge-shared octahedra is not a perovskite. The structure difference will give rise to different electronic structures, which in turn will affect the optical absorption. While this paper measured the optical band gap, the absolute absorption coefficient was not measured. So, whether it can be suitably used for PV is still unclear. The 1.1 eV band gap is already close to the lower bound of the optimal range for a single-junction solar cell. If the fundamental gap is significantly lower than the optical band gap, it will limit the open circuit voltage to a low value.

Is the work clearly and accurately presented and does it cite the current literature?
Yes

Is the study design appropriate and does the work have academic merit?
Yes

Are sufficient details of methods and analysis provided to allow replication by others?
Yes

If applicable, is the statistical analysis and its interpretation appropriate?
Yes

Are all the source data underlying the results available to ensure full reproducibility?
Yes

Are the conclusions drawn adequately supported by the results?
Yes

Competing Interests: No competing interests were disclosed.

Reviewer Expertise: First-principles calculations, Raman spectrum

I confirm that I have read this submission and believe that I have an appropriate level of expertise to confirm that it is of an acceptable scientific standard.

Author Response 18 May 2023

Rokas Kondrotas

Reviewer #2

It is enjoyable to read through this paper, which reports the synthesis and characterization of the compound SnZrSe3, an unknown material so far. Even though SnZrSe3 appears to be

isostrutural to SnZrS3, it is an important addition to the database of inorganic crystals. The description on the experimental details and the discussion on the results are detailed and objective enough to assure the reader what has been done and what still requires further study. I have no reservation regarding the indexing of this work. Nevertheless, given the complete open nature of this journal, I would like to add a discussion which might be of interest to the readers of this paper.

Reviewer: The "perovskite" structure, without any generalization, should be composed of corner-shared octahedra. In this sense, the ribbon-like structure of SnZrSe3 with edge-shared octahedra is not a perovskite. The structure difference will give rise to different electronic structures, which in turn will affect the optical absorption. While this paper measured the optical band gap, the absolute absorption coefficient was not measured. So, whether it can be suitably used for PV is still unclear. The 1.1 eV band gap is already close to the lower bound of the optimal range for a single-junction solar cell. If the fundamental gap is significantly lower than the optical band gap, it will limit the open circuit voltage to a low value.

Authors: we thank the reviewer for positive feedback and raising awareness. The ideas that are expressed are very important and deserves a discussion. While providing a response to reviewer #1, some of the concerns have been discussed, and is added in the version 2 of the paper. In particular, the following discussion have been added to account for change in optical properties with respect to crystal structure: On one hand, absorption coefficient (α) depends on the density of states in the bands. If states at direct gap are dispersive it can lead to slowly increasing α resulting in significant absorption onset. Based on optical properties calculated for $SnZrSe_3$, α > 104 cm-1 is reached for photon energy > 1.5 eV which renders an onset of around 0.9 eV[18]. Another theoretical work also shows that among ABX3 chalcogenides those in needle-like phase have a larger absorption onset than those in perovskite structure[12], and this was measured for $SrZrS_3$ case experimentally [R1]. On the other hand, in materials with dispersive bands, a high carrier mobility can be expected. Consequently, for practical application, for instance solar cells, an optimum absorber thickness will be required to balance between charge carrier mobility, lifetime and absorption coefficient.

Reference: R1: https://doi.org/10.1002/adma.201604733

Competing Interests: No competing interests were disclosed.

Reviewer Report 31 January 2023

https://doi.org/10.21956/openreseurope.16407.r30579

© 2023 Zeng H. This is an open access peer review report distributed under the terms of the Creative Commons Attribution License, which permits unrestricted use, distribution, and reproduction in any medium, provided the original work is properly cited.

Hao Zeng
Department of Physics, University at Buffalo, Buffalo, NY, USA

This paper reports the synthesis of chalcogenide perovskite SnZrSe3, using solid state reaction. Very rarely has selenide perovskite been synthesized and their physical properties characterized. While the method used is not entirely novel, the results will be of great interest to the community working on chalcogenide perovskites. The paper is suitable for indexing after the authors address the following comments:

1. The authors stated that "However, other ABX_3 chalcogenides although having a non-perovskite ground phase, are also stable compounds, have bandgaps in the infrared region and have high optical absorption." This is not entirely true. The hexagonal (indirect gap) and need-like phases (pseudo-direct gap) has weaker light absorption than that of the perovskite phase. See Sun's Nano Lett paper (Ref. 12).

2. In this work, single phase perovskite was not achieved. Instead a mixture of binary phases including ZrSe3, ZrSe2 and SnSe were present. The authors should discuss if there is a pathway towards realizing phase pure materials. Without it the impact of the work is significantly limited.

3. It was shown that when the ampoule was oriented horizontally no secondary Sn-related phases were observed. What happens if excess Sn precursor is used? If there is no secondary phase, what happens to excess Sn?

4. It is stated that first-principles calculations are known to underestimate the bandgap. This is also not true. For example HSE predicted band gaps often are consistent with experimental results and GW sometimes tend to overestimate band gap.

5. It is stated that n-type samples are slightly more Se-rich. However, selenium vacancy should contribute to excess electron carriers. For Se-rich samples, where do excess electrons come from, if not from secondary phase or contaminations? Moreover, how does perovskite accommodate excess Se, unless they occupy cation sites? Such antisite defects are shown to have too high formation energy. Moreover, composition analysis seems to show that the samples are Se deficient (< 60%).

6. Presence of oxygen can lead to apparently higher band gap measured from UV-vis spectroscopy. Can the authors rule out presence of oxygen as the source of their apparently larger band gap than expected?

7. The authors should be careful on claiming presence of both n- and p-type doping, unless they can be sure secondary phases/contaminations are irrelevant. If n- and p-type behavior is indeed attributed to SnZrSe3, defects/dopants should be identified. Furthermore, while authors pointed out that chalcopyrites are often p-type due to Cu vacancies, they failed to mention that both n- and p-type behavior has already been realized in chalcogenide perovskite BaZrS3 using gating. see Yu *et al*, Nano Energy, 85, 105959[1].

8. The authors stated that "$SnZrSe_3$ is predicted to have a small (< 0.1 eV) difference between indirect and direct gaps as well. Such characteristic is highly desired in absorber materials for photovoltaics because high absorption coefficient and long carrier lifetime can be

realised simultaneously". Does the theory paper they cited and their own measurement results support this statement? In ref 18, it showed that the onset of absorption is at least .5 eV higher than the predicted band gap. Their own measurements also showed that significant absorption is only available at > 1.5 eV. What is the nature of the direct and indirect gap states? If the direct gap states are dispersive, they will not have high absorption. The authors should put this into perspective by comparing to existing materials (either the calculated dielectric constant or measured absorption coefficient).

References

1. Yu Z, Wei X, Zheng Y, Hui H, et al.: Chalcogenide perovskite BaZrS3 thin-film electronic and optoelectronic devices by low temperature processing. *Nano Energy*. 2021; **85**. Publisher Full Text

Is the work clearly and accurately presented and does it cite the current literature?
Yes

Is the study design appropriate and does the work have academic merit?
Yes

Are sufficient details of methods and analysis provided to allow replication by others?
Yes

If applicable, is the statistical analysis and its interpretation appropriate?
Not applicable

Are all the source data underlying the results available to ensure full reproducibility?
Yes

Are the conclusions drawn adequately supported by the results?
Partly

Competing Interests: No competing interests were disclosed.

Reviewer Expertise: Chalcogenide perovskites, optoelectronic properties.

I confirm that I have read this submission and believe that I have an appropriate level of expertise to confirm that it is of an acceptable scientific standard, however I have significant reservations, as outlined above.

Author Response 18 May 2023

Rokas Kondrotas

Reviewer #1 This paper reports the synthesis of chalcogenide perovskite SnZrSe3, using solid state reaction. Very rarely has selenide perovskite been synthesized and their physical properties characterized. While the method used is not entirely novel, the results will be of great interest to the community working on chalcogenide perovskites.

Authors: first of all, we thank reviewers for on point comments and raised questions. In the following report we have addressed these questions as accurate as possible and updated the publication as provided herein.

Reviewer: The paper is suitable for indexing after the authors address the following comments:

The authors stated that "However, other ABX3 chalcogenides although having a non-perovskite ground phase, are also stable compounds, have bandgaps in the infrared region and have high optical absorption." This is not entirely true. The hexagonal (indirect gap) and needle-like phases (pseudo-direct gap) has weaker light absorption than that of the perovskite phase. See Sun's Nano Lett paper (Ref. 12).

Authors: We do agree with a comment made. To avoid ambiguity and present potential drawbacks having a non-perovskite type ABX_3 materials, we modified this part of introduction as follows: Other ABX_3 chalcogenides although in a non-perovskite ground phase have bandgaps spanning from near to mid-wavelength infrared regions[12]. Additionally, because valence and conduction bands in edge(face)-sharing ABX_3 chalcogenides is primarily determined by p and d orbitals of X and B elements, respectively, the absorption coefficient is expected to be high as well [R1.1]. Note, however, that lower symmetry crystal structures such as needle-like or $BiNiO_3$-type can lead to indirect optical transitions and therefore higher absorption onset as compared with ABX_3 chalcogenides in perovskite-type structure. Reference: R1.1. https://doi.org/10.1021/acs.inorgchem.8b01038

Reviewer: In this work, single phase perovskite was not achieved. Instead a mixture of binary phases including ZrSe3, ZrSe2 and SnSe were present. The authors should discuss if there is a pathway towards realizing phase pure materials. Without it the impact of the work is significantly limited.

Authors: when working with this material, indeed we were not able to achieve high yield of $SnZrSe_3$ phase. Traditionally, in a solid-state synthesis one focuses on finding optimal temperature and ensuring that precursors are evenly distributed through regrinding and mixing steps. Meanwhile duration of the annealing process was not taken into account having a perception that the longer process - the better. While continuing our work on the synthesis optimisation we noticed an interesting feature. Samples that were annealed for a shorter duration had higher yield of $SnZrSe_3$ phase. So we made additional experiments where only duration process was varied and found that shorter durations than we typically used for our process yielded a higher concentration of $SnZrSe_3$ phase. Having these new insights in the experiment we have updated the publication as follows: *-Slightly corrected the experimental section to include new annealing parameters:* Ampoules were introduced in the tube furnace, 13 of them in a horizontal and 3 of them in a vertical (placed in ceramic holder) positions at the centre of the heating zone. The heating process included either one or two steps: (i) temperature was raised to the top temperature within 3 – 7 h which was varied in the 600 – 800 °C range and held for 10 – 80 h; (ii) in the second step, the temperature was reduced to 100 – 600 °C within 7 – 60 h, and furnace power was switched off leaving to cool down naturally for a few hours. We found that larger crystals were

formed when the temperature was reduced slowly in the second stage, instead of maintaining a high furnace temperature for a prolonged period of time. Note: initially we presented that annealing at top temperature was held for 10 – 80 h, which suggests that we tested short annealing durations. However, a short duration was used in two-step annealing process where in the second step temperature was slowly (~0.03 ^{o}C/min) reduced. Therefore, technically duration at the crystallization temperature range was 60 – 80 h. - *Rewritten first paragraph about solid state synthesis as follows:* $SnZrSe_3$ was synthesized via solid state reaction from precursors in elemental form. Unless stated otherwise, a transport agent (SnI_2) was used to accelerate the reaction and to grow single crystals. In other cases, no additives were introduced. In most of experiments, various shapes, sizes and forms of crystals were present inside an ampoule after annealing indicating formation of secondary phases. By analysing XRD data we found that in addition to $SnZrSe_3$ phase, one or two of the following binary phases were present: $ZrSe_3$ (ICDD# 03-065-2351), $ZrSe_2$ (ICDD# 04-005-5128) and SnSe (ICDD# 04-009-2257). Based on multiple trials, we noticed that the following experimental parameters had a deciding factor on the phase composition: (i) spatial separation of precursor materials (ii) Se overpressure in the ampoule and (iii) annealing duration. When the ampoule was oriented vertically in the annealing zone, $ZrSe_3$ and traces of SnSe phases were present despite the annealing temperature applied (Figure 1a). Interestingly, the addition of transport agent in a form of SnI_2 did not change the phase composition. This suggested that when precursors were in close proximity, the solid-state reaction was not accelerated or favoured for the formation of $SnZrSe_3$ in the presence of a transport agent. When ampoules were oriented horizontally and precursor powder was spread over a certain length, phase composition strongly depended on the initial Se content. Using Se-deficient precursor, a large amount of $ZrSe_2$ and absence of $ZrSe_3$ phases were observed in the powder (Figure 1b). Once stoichiometric or Se-rich precursors were used, little to no amount of $ZrSe_2$ was found, which indicated that the formation of $ZrSe_3$ phase was highly favoured under Se-rich atmosphere. Note that when the ampoules were oriented horizontally no secondary Sn-related phases were observed. Finally, the annealing duration at the top temperature had a significant effect on $SnZrSe_3$ powder phase purity. In the initial experiments we used long annealing durations to facilitate a complete solid-state reaction. However, we noticed that shorter annealing durations yielded lower concentration of secondary phases (Figure 1 c). In the samples annealed under identical conditions but with different durations, we found that almost pure-phase powder was obtained annealing for 35 h instead of 60 h or more used previously (Figure 1c). Longer or shorter than 35 h annealing durations resulted in the formation of $ZrSe_2$ phase which concentration was much higher in the sample synthesized for a long period of time. This suggested that $SnZrSe_3$ formed relatively quickly and under prolonged annealing time slowly decomposed into binary phases. Therefore, from these results we can infer that 700 ^{o}C is close to the decomposition temperature of $SnZrSe_3$. - *Modified final paragraph about solid-state:* Therefore, we believe that the thermodynamic balance between reactions (3) and (4) which depends on spatial separation of materials, partial Se pressure and annealing temperature determine the final product composition. While inspecting the ampoule annealed sequentially first at 700 °C and then at 800 °C, it was noticed that after the second annealing large $SnZrSe_3$ crystals deteriorated, and small fine needle-like crystals typical for $ZrSe_3$ were found (Figure S1 in Extended data[22]). This indicated that $SnZrSe_3$ decomposes at higher temperatures. This observation was in agreement with the results obtained from time-dependent annealing series, where prolonged synthesis duration at 700 °C led to

decomposition of $SnZrSe_3$. Therefore, to synthesize $SnZrSe_3$ phase with high yield, it is essential to keep balance between top temperature and annealing duration. With our experimental setup it was around 35 h at 700 °C. However, if lower temperature is applied, longer duration may be required and vice versa.

Updated Figure 1 by adding powder patterns of samples synthesized for different annealing durations: Figure 1. (a) Diffractograms of $SnZrSe_3$ powder synthesized at various temperatures in a vertical position without and with transport agent. (b) Diffractograms of $SnZrSe_3$ powder samples synthesized in the same experiment at 740 °C temperature in a horizontal position with different initial Se-content in the precursor as indicated in the graph. (c) Diffractograms of $SnZrSe_3$ powder annealed for different durations. Top temperature – 700 °C, SnI_2 transport agent, position – horizontal, composition - stoichiometric. (d) XRD pattern of collected and grinded crystals synthesized at 700 °C in horizontal position with a transport agent. Diffractogram of pure $SnZrSe_3$ phase was simulated using CIF file (underlying data [22]).

Reviewer: In It was shown that when the ampoule was oriented horizontally no secondary Sn-related phases were observed. What happens if excess Sn precursor is used? If there is no secondary phase, what happens to excess Sn?

Authors: that is a valid point which we were asking ourselves too. Naturally, if we have a decomposition or incomplete reaction of binary phases we should be able to observe both Zr-related and Sn-related secondary phases. This, however, was not always the case. We are not entirely certain about the mechanism, but a current hypothesis is as follows: Sn-related phases were not observed in samples when horizontal configuration was used or higher than 700 ^{O}C temperature applied. In these ampoules, at the very end of ampoule (photo below), optically we observed condensation of material which had a mixture of metallic and red lustre. Usually, this part material was not collected for analysis because of difficulty to scratch it off from uneven quartz ends and was assumed to be condensate of transport agent. However, in few samples we have carried out chemical analysis of these droplets and found elements Sn, Se and I. This suggested that not only transport agent but also some Sn-Se phase condensed on ampoules ends. At high temperature (> 700 ^{O}C) all SnSe whether as a product of decomposition or incomplete reaction is likely in vapour phase and with a help of iodine is transferred to the coldest part of ampoule. Very likely this occurred during cool down step. So our primary explanation is that excess of Sn condensed on the very ends of ampoules and was not collected (Figure 2).

Reviewer: It is stated that first-principles calculations are known to underestimate the bandgap. This is also not true. For example HSE predicted band gaps often are consistent with experimental results and GW sometimes tend to overestimate band gap.

Authors: we do agree with reviewer's comment on the first principal high accuracy in predicting bandgap using hybrid functionals such as HSE06. The discrepancy we found in experimentally measured bandgap and the one calculated using mBJ (potential that also produces bandgaps consistent with experiments) was quite large i. e. 1.1 eV (exp) vs 0.53 eV (calc). We could argue that our experimental way of defining bandgap (using diffuse reflectance) could potentially not account for weak indirect optical transitions, and that real

indirect bandgap would be within error of calculated value. But based on the band structure the difference between direct and indirect gaps in $SnZrSe_3$ and $SnZrS_3$ is < 0.1 eV [T7]. This therefore cannot account for a large difference (> 0.5 eV) between experimental and calculated values. Note that this discrepancy is more pronounced for needle-like ABX_3 chalcogenides as shown in the Table 1 below. Based on this we conclude that needle-like phase ABX_3 chalcogenides are less accurately described in DFT than perovskite or hexagonal phases. Additionally, in $SnZrSe_3$ there exist a lone electron pair of Sn, which can further complicate high accuracy simulations using DFT.

Table 1. Bandgaps of selected ABX_3 chalcogenides determined experimentally and calculated using first principals. Compound Structure Exp E_g, eV Calc* E_g, eV ΔEg, eV Ref. $SrZrS_3$ DP 2.13 1.95 0.18 [T1] $SrZrS_3$ **N** 1.53 1.17 **0.36** [T1] $BaZrS_3$ DP 1.81 1.75 0.06 [T1] $BaTiS_3$ H 0.27** 0.16 0.11 [T2] $SrTiS_3$ H 0.25** 0.25 0.0 [T3] $SrHfS_3$ DP 2.32 2.28 0.06 [T4] $BaHfS_3$ DP 2.06 2.0 0.06 [T4] $SrHfSe_3$ **N** 1.02 0.79 **0.24** [T5] $SnZrSe_3$ **N** 1.10 0.63 **0.47** This work DP – distorted perovskite structure, prototype $GdFeO_3$ N – needle-like structure, prototype NH_4CdCl_3 H – hexagonal structure, prototype $BaNiO_3$ * - all calculated values are taken from the work of Sun et al. [T6], except for $SnZrSe_3$ [T7]. Reference is provided for experimentally determined bandgap values. ** - absorption edge.

Taking the comments into account, we have modified the discussion part regarding calculated and observed bandgaps as follows: First-principles calculations using hybrid potentials can predict bandgaps consistent with experimental values therefore such large discrepancy we relate to one of the two reasons: (i) $SnZrSe_3$ is an indirect bandgap semiconductor and using diffuse reflectance method we were not able to clearly detect weak indirect optical transitions which would be expected to be lower in energy than direct (ii) due to low density of states at the band edges, strong optical absorption starts with an high onset leading significant absorption only at higher photon energies [18].

References: T1. https://doi.org/10.1002/adma.201604733 T2. https://doi.org/10.1038/s41566-018-0189-1 T3. https://doi.org/10.1021/acs.chemmater.8b02279 T4. https://doi.org/10.1021/jacs.8b13622 T5. https://doi.org/10.1021/acs.inorgchem.8b01038 T6. https://doi.org/10.1021/nl504046x T7. https://doi.org/10.1016/j.mtcomm.2021.102427

Reviewer: It is stated that n-type samples are slightly more Se-rich. However, selenium vacancy should contribute to excess electron carriers. For Se-rich samples, where do excess electrons come from, if not from secondary phase or contaminations? Moreover, how does perovskite accommodate excess Se, unless they occupy cation sites? Such antisite defects are shown to have too high formation energy. Moreover, composition analysis seems to show that the samples are Se deficient (< 60%).

Authors: first, we would like to clarify that when we used the term “more Se-rich” we meant Se content when comparing samples with each other, but not with expected ABX_3 stoichiometric composition 1:1:3. We have clarified this as follows: In both samples, the cationic ratio A/B was identical, whereas the n-type crystal was slightly more Se-rich than p-type, but both were Se-deficient with respect to stoichiometric ratio of [X]/([A]+[B]) which is 1.5. All samples which we have analysed can be considered as Se-deficient and cation-rich

with respect to an ideal 1:1:3 ratio. In terms of atomic percentage of Se it was always found to be in 57 – 58.5 at.% range. If high oxygen contamination was present, even lower Se concentration was found. However, even for very clean as-grown crystals measured immediately after synthesis where no oxygen was present, the Se content was no more than 58.5 at.%. There are two possible reasons for this observation: (i) deviation could be related to the high measurement system error (> 2 at.%). Although this is unlikely because using the same conditions we measured the composition of GaAs, GeS, GeSe monocrystals on the same system and all them showed a 50:50 atomic ratio with 0.5 at.% error. Another reason could be that a equilibrium composition of $SnZrSe_3$ is not 1:1:3, but slightly cation-rich and anion-deficient such as: 1.05 : 1.05 : 2.9. In fact, other ABX_3 chalcogenides in needle-like or hexagonal phases were also found not to follow 1:1:3 ratio strictly, e. g. $Ba_{1.12}Zr_{1.0}Se_{3.01}$, $Sr_{21}Ti_{19}Se_{57}$ [R5.1] or $Sn_{1.2}Ti_{.08}S_3$ [R5.2] $Ba_{1.06}Ti_1S_{2.95}$ [R5.3]. Thus it is not known for certain what is the precise equilibrium stoichiometry of $SnZrSe_3$ compound and at which point it can be regarded as Se-rich or Se-poor. Therefore, in our work we focused on comparing and finding trends within sample series rather than with absolute values. Additionally, we have strong evidence that cations play more important role than anion in defect chemistry related to conductivity on which we elaborated more in question 7. Because of the reasons outlined above, the discussion about Se-vacancy defects as potential donors becomes speculative. Although we cannot completely rule out the contribution of V_{Se}, there is a stronger correlation of conductivity type and carrier concentration with cation composition.

References: R5.1. https://doi.org/10.1021/ja972442p R5.2. https://doi.org/10.1063/1.5093183 R5.3. https://doi.org/10.1038/s41566-018-0189-1 (in supporting information)

Reviewer: Presence of oxygen can lead to apparently higher band gap measured from UV-vis spectroscopy. Can the authors rule out presence of oxygen as the source of their apparently larger band gap than expected?

Authors: we agree that oxygen if incorporated in the lattice and resulting in formation of $SnZr(Se,O)_3$ alloy would lead to higher than expected bandgap as was observed in [R6.1]. However, there are two reasons why we think oxygen had no contribution in optical absorption in our case: (i) first powder sample that were used to measure bandgap was obtained by grinding needle-shaped crystals. Compositional analysis of the crystals usually showed no content or very minor traces of oxygen. Higher content of oxygen was observed when crystals were grounded to powder and exposed for prolonged time under ambient. This shows that during synthesis process there was no contamination with oxygen, and it was not incorporated in the lattice. It is very unlikely that at room temperature oxygen from air would be incorporated into the crystal lattice of $SnZrSe_3$ and lead to formation of $SnZr(Se,O)_3$. (ii) Another evidence that oxygen does not enter $SnZrSe_3$ lattice is based on the lattice parameters of $SnZrSe_3$. If oxygen was incorporated in the crystal lattice, the lattice parameters of $SnZrSe_3$ would shrink because of much smaller ionic radius of O than Se. In the following Table 2 we present lattice parameters calculated for one of our $SnZrSe_3$ powder:
Table 2. Lattice constants of $SnZrSe_3$ Sample a, Å b, Å c, Å As synthesized 9.5940 3.8463 14.4087 Aged 7 months 9.5936 3.8462 14.4082 Single crystal 9.5862 3.8443 14.3959

It is quite clear that lattice constants do not change with time indicating there is no change in $SnZrSe_3$ lattice under ambient conditions, and that lattice parameters calculated for powder sample is slightly higher than measured in single crystal. If oxygen was incorporated in the lattice, there would be a much more significant shift of lattice constants and toward smaller not higher values. Reference: R6.1.
https://doi.org/10.1021/acs.jpclett.1c00177

Reviewer: The authors should be careful on claiming presence of both n- and p-type doping, unless they can be sure secondary phases/contaminations are irrelevant. If n- and p-type behavior is indeed attributed to SnZrSe3, defects/dopants should be identified. Furthermore, while authors pointed out that chalcopyrites are often p-type due to Cu vacancies, they failed to mention that both n- and p-type behavior has already been realized in chalcogenide perovskite BaZrS3 using gating. see Yu et al, Nano Energy, 85, 1059591.

Authors: we do agree that claims about n- and p-type doping engineering in $SnZrSe_3$ based on intrinsic defects lack more evidence therefore we acknowledged a possible contribution of impurities in the following part: **"**Important to note that since iodine was used as a transport agent to facilitate the solid state reaction during synthesis, it could be inadvertently introduced in the lattice giving rise to extrinsic doping. Iodine could not be detected by EDX, but we acknowledge that very small amounts (beyond the EDX detection limit) can have a significant contribution to the conductivity behaviour." Because single crystals were used for electrical measurements, we are quite certain that there is no contribution to conductivity from secondary phases. Secondly, because we were able to observe p-type conductivity, we can be sure, that p-type can be achieved to some extent by modifying $SnZrSe_3$ composition alone. Finally, although extrinsic doping via iodine impurities is possible, in chalcogenides doping of halogens usually introduce shallow donor defects, e.g. ZnSe:I E_a = 0.026 eV [R7.2], SnS:Cl E_a=0.0015 eV [R7.3], Sb_2Se_3:Br E_a=0.06 eV (calculated) [R7.4]. Therefore, despite whichever sample we test, we should be able to observe additional probably low activation energy in the conductivity vs temperature graph. This was not the case. So we strongly believe that n- and p-type doping originated from intrinsic $SnZrSe_3$ defects. To identify which point defects are responsible for generating free electrons/holes is very difficult without knowledge of defect chemistry in $SnZrSe_3$ on theoretical basis. This is our initial work on $SnZrSe_3$ and in the future it would be extremely useful to analyse defect chemistry from first-principles. This then would allow us to identify potential free carrier generating defects. Additionally, currently we are working of the synthesis of $Sn(Zr_{1-x}Ti_x)Se_3$ alloy system and observed a very strong correlation between change of resistivity (5 orders of magnitude) and Ti content which again points to the fact that cations rather than anion or extrinsic doping is more critical to electrical behaviour of $SnZrSe_3$. Regarding the achievements in observing both type carriers in $BaZrS_3$, this is indeed an important milestone and this publication was added in the main text: In this work, we found that $SnZrSe_3$ showed *p* as well as *n* type conductivity behaviour. Ambipolar behaviour was also recently realised in $BaZrS_3$ thin films [R7.1].

Reference R7.1. https://doi.org/10.1016/j.nanoen.2021.105959 R7.2. https://doi.org/10.1016/0022-0248(88)90607-0 R7.3. https://doi.org/10.1021/acs.cgd.0c00617 R7.4. https://doi.org/10.1021/acsaem.9b02192

Reviewer: The authors stated that "SnZrSe3 is predicted to have a small (< 0.1 eV) difference between indirect and direct gaps as well. Such characteristic is highly desired in absorber materials for photovoltaics because high absorption coefficient and long carrier lifetime can be realised simultaneously". Does the theory paper they cited and their own measurement results support this statement? In ref 18, it showed that the onset of absorption is at least .5 eV higher than the predicted band gap. Their own measurements also showed that significant absorption is only available at > 1.5 eV. What is the nature of the direct and indirect gap states? If the direct gap states are dispersive, they will not have high absorption. The authors should put this into perspective by comparing to existing materials (either the calculated dielectric constant or measured absorption coefficient).

Authors: Regarding the first question, we do not have estimates of carrier lifetime therefore we cannot fully support the statement. Whether bands are dispersive we can only rely on ref 18 results, which suggest that it strongly depends on the crystallographic direction. Near the indirect gap region bands are indeed flat which would suggest high optical absorption, whereas in other directions they are dispersive, e.g. Γ→ R (figure below). Note that in ref 18 only the calculated values of absorption coefficient are presented. However, we do acknowledge that larger absorption onset was observed in ABX_3 chalcogenides of needle-like phase and therefore extent the discussion in the manuscript as follows: On one hand, absorption coefficient (α) depends on the density of states in the bands. If states at direct gap are dispersive it can lead to slowly increasing α resulting in significant absorption onset. Based on optical properties calculated for $SnZrSe_3$, $\alpha > 10^4$ cm^{-1} is reached for photon energy > 1.5 eV which renders an onset of around 0.9 eV[18]. Another theoretical work also shows that among ABX_3 chalcogenides those in needle-like phase have a larger absorption onset than those in perovskite structure[12], and this was measured for $SrZrS_3$ case experimentally [R8.1]. On the other hand, in materials with dispersive bands, a high carrier mobility can be expected. Consequently, for practical application, for instance solar cells, an optimum absorber thickness will be required to balance between charge carrier mobility, lifetime and absorption coefficient.

Electronic band dispersion curves of $SnZrSe_3$ along high symmetry direction of the Brillouin zone. Adapted from ref.18. Reference: R8.1: https://doi.org/10.1002/adma.201604733

Competing Interests: No competing interests were disclosed.